Potential of GPS common clock single-differences for deformation monitoring

S. Schön, H. K. Pham, T. Kersten,
Institut für Erdmessung
Leibniz Universität Hannover, Schneiderberg 50, D-30167 Hannover, Germany

J. Leute, A. Bauch
Physikalisch-Technische Bundesanstalt, Bundesallee 100, D-38116 Braunschweig, Germany

Abstract. Global satellite navigation systems (GNSS) are a standard measurement device for deformation monitoring. In many applications, double-differences are used to reduce distance dependent systematic effects, as well as to eliminate the receiver and satellites clock errors. However, due to the navigation principle of one way ranging used in GPS, the geometry of the subsequent adjustment is weakened. As a result, the height component is generally determined three times less precisely than the horizontal coordinates. In addition, large correlations between the height and elevation dependent effects exist such as tropospheric refraction, mismodelled phase center variations, or multipath which restricts the attainable accuracy. However, for a kinematic analysis, i.e. for estimating high rate coordinate time series, the situation can be significantly improved if a common clock is connected to different GNSS receivers in a network or on a baseline. Consequently, between-station single-differences are sufficient to solve for the baseline coordinates. The positioning geometry is significantly improved which is reflected by a reduction of the standard deviation of kinematic heights by about a factor 3underlining the benefits of this new approach.. Real data from baselines at the Physikalisch-Technische Bundesanstalt campus at Braunschweig where receivers are connected over 290 m via an optical fiber link to a common clock was analysed.

Keywords. GPS, Monitoring, Clock Modeling, Common Clock, EMRP JRP SIB60

1 Introduction

GNSS are widely applied for continuous monitoring tasks, such as e.g., for bridges (Roberts et al. 1999, Wieser and Brunner 2002), tall buildings (Lovse et al. 1995, Li et al. 2005), landslides (Malet et al. 2002, Schön et al. 2005, Brückl et al. 2013), earthquakes (Larson 2009, Avallone et al. 2011), or open pit mines (Kim et al. 2003). A kinematic processing of the observation data enables high temporal resolution of the coordinate time series allowing the study of fast small motions of tall buildings or earthquakes (Weinbach and Schön 2015). Currently, data rates of up to 100 Hz are used to investigate vibrations, Mochas and Stiros (2013), Xu et al. (2012). Partially, the results are suffering from the latency and amplitude overshoot of the high rate GNSS receivers, cf. Bischof and Schön (2013) or Häberling et al. (2015).

However, the attainable accuracy and precision of kinematic height time series is limited by high physical correlations between the parameters, namely height, tropospheric delay, and explicit or eliminated receiver clock parameters (i.e. the latter in case of double-differences (DD)), Weinbach (2013). As a result, typically three-times larger noise of the height compared to the horizontal coordinate components is obtained masking valuable small patterns in the time series, see e.g. Weinbach and Schön (2015) for the case of an earthquake.

Benefitting from modern ultra stable atomic clocks, this situation can be significantly improved by estimating the receiver clock error in a physically meaningful way, i.e. over longer intervals instead of the classical epoch wise estimation or equivalently epochwise elimination by DD. Current results for this clock modeling approach can be found in Weinbach (2013), Wang and Rothacher (2014) and Weinbach and Schön (2015) for precise positioning with carrier phase observations or Krawinkel and Schön (2015) for navigation with code observations.

For relative positioning, so-called common clock set-ups have been proposed in order to improve the results. In this case, an external clock signal is fed into the receivers by a very stable link and between-station single-differences (SD) are processed instead of DD, since both receiver clocks are supposed to be perfectly synchronized.

From a theoretical point of view, Santerre and Beutler (1993) showed that processing SD will outperform a DD approach for static positioning w.r.t. the accuracy and precision of the results. At that time, they proposed a GPS receiver design with multiple antenna inputs and one common board. Their simulation study showed an expected improvement of the height standard deviation by a factor of up to 5. Concerning the systematic effects, they emphasized the amplification of remaining tropospheric errors by a factor of 2.6 - 4.2 for the coordinate domain, when coordinates and epoch-wise receiver clock errors are estimated or eliminated by forming DD. In case of perfect synchronization a smaller impact of 1.9 - 2.2. is reported.

Macias-Valadez et al. (2010) revisited this idea and built a corresponding multi antenna GPS over fiber measurement set-up. Here, each antenna is equipped with a front end ("remote station"). The frequency of one common local oscillator is transported via (2 km) fibre to the front end and used to downconvert the GPS signal to an intermediate frequency (IF) level. Afterwards this GPS IF is transmitted by optical fiber to the common receiver. Macias-Valadez et al. measure precisely the relative hardware delay variations between the fibre links in real time. For zero and short baselines a high precision of 4 mm, comparable to those of the horizontal coordinates could be achieved. However, most of the installation was inside the laboratory with a baseline of only 1 m.

It turned out that a perfect receiver clock synchronization below the expected phase noise level (e.g. 1 mm) is still a big challenge. The temperature influence of 175 ppm/°C for RG58 RF cables that are often used to connect antennas or clocks yields easily differential delays at the mm-level. This is supported by our own results from common clock setups realised by fiber optics between actual separated pillars (290 m) at the Meitner and Kopfermann building at Physikalisch-Technische Bundesanstalt (PTB, Braunschweig, Germany). The set-up was operated in the context of the research “Surveying” project, undertaken in the context of the European Metrology Research Program (EMRP), Pollinger et al. (2015).

In this contribution, we will relax the severe synchronization requirements. Based on experiments carried out at PTB, we will show that a common clock SD approach can significantly improve *kinematic* height residuals even if a perfect synchronization at the 1 mm level between the receivers cannot be obtained due to environmental variations, such as e.g., temperature variations and their impact on receiver, antenna, and clock cable.

The remainder of the paper is structured as follows. In section 2, the measurement set up is described. Next, the clock modeling approach for the kinematic processing of common clock SD is presented. The improvements to be expected were analyzed by simulations with different processing schemes. Finally, real data are analysed, the improvements underlined and potential applications for GNSS based monitoring are discussed.

2 Measurement Set-up

GNSS data are collected at PTB campus in October 2013. The stations at the Meitner building (MEI1 and MEI2) are free of obstructions down to 0° elevation angle and the antennas are located above the trees/forest at the PTB campus. The posts MEI1 and MEI2 are at the same height and separated by approximately 5 m. KOP1 is located approximately 16 m below and 290 m away from MEI1 in the forest, yielding obstructions up to elevations of 25°. Fig. 1 shows the station environment and the experimental set up.

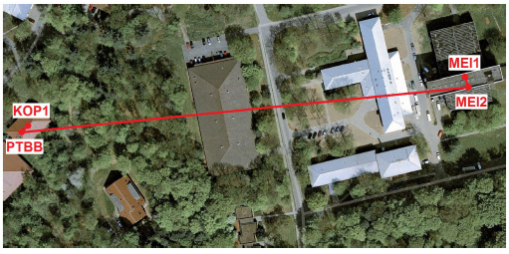

(a)

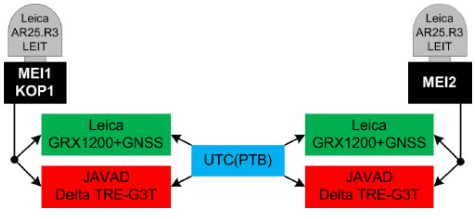

(b)

Fig. 1 Measurement set up a) aerial photograph of the PTB campus and the three stations involved b) common-clock receiver/antenna set-up.

Leica AR 25 (Rev. 3) antennas individually and absolutely calibrated at Institut für Erdmessung (IfE) Hannover were mounted at both endpoints of the baselines, (i) the short 5 m baseline MEI1-MEI2 and (ii) the longer 290 m baseline KOP1-MEI2. At each side, two different receivers (Javad Delta and Leica GRX1200) were operated in parallel, in order to analyse the impact of different receiver types. A unique, H-maser quality signal UTC(PTB) is fed to all receivers via fiber optic cable ensuring a "common clock" set up.

The observation period lasted from October 16 to October 29, 2013 (DOY289-DOY302) with a data rate of 1 sec. As an example, Fig. 2 shows an overview of the signal quality in terms of the carrier to noise density for each satellite for DOY 297 in 2013. The comparison shows the reduced signal strength (blue colors) at low elevation angles for the Kopfermann building, induced by signal diffraction and partial obstructions by trees and foliage.

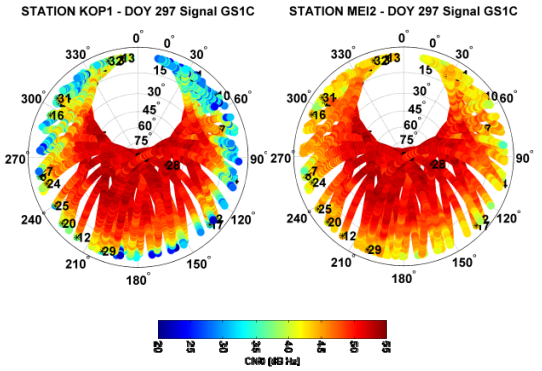

Fig. 2 Skyplots with color-coded carrier to noise density ratios, for the Kopfermann (left) and Meitner building (right), respectively. A common color scale is applied. Blue colors indicate weak signals

3 Concept of Kinematic Positioning with Common Clock Single-differences

3.1 Observation Equation

The observation equation for the GPS carrier phase Φ_A^k between satellite k and station A reads:

$$\Phi_A^k = \rho_A^k + c\left(\delta t_A - \delta t^k\right) - I_A^k + T_A^k + \lambda N_A^k + \varepsilon_A^k \quad (1)$$

where ρ_A^k denotes the geometric range, $c\delta t_A$ and $c\delta t^k$ the metric receiver and satellite clock error, respectively, including hardware and cable delays, I_A^k the ionospheric delay, T_A^k a tropospheric delay, λN_A^k the metric ambiguity and ε_A^k residual errors, such as e.g., antenna phase center variations or multipath and noise.

A similar observation equation can be formed for station B and subsequently between-station SD_{AB}^k and DD_{AB}^{kl} can be computed

$$SD_{AB}^k = \rho_{AB}^k + c\delta t_{AB} + T_{AB}^k + \lambda N_{AB}^k + \varepsilon_{AB}^k \quad (2a)$$

$$DD_{AB}^{kl} = \rho_{AB}^{kl} + T_{AB}^{kl} + \lambda N_{AB}^{kl} + \varepsilon_{AB}^{kl} \quad (2b)$$

A kinematic, epochwise estimation of the receiver coordinates of station B w.r.t. station A is computed in order to monitor variations of the baseline length between both stations. In a standard approach, DD will be used in order to eliminate any type of receiver clock error and further reduce the error budget of distance dependent effects. In our case, however, we will take benefit of the common-clock assembly, i.e. the differential receiver clock error between the two stations cannot vary in an arbitrary way, since a common clock signal of a stable clock is fed to the receivers via a high quality fiber optic cable link. A constant (initial) offset between the receivers' clocks will persists as well as small few mm variations due to temperature variations in the cables and hardware (Ray and Senior, 2003), as discussed in sec. 5.1.

3.2 Common Clock Processing Model

In the concept of receiver clock modeling proposed and successfully applied by Weinbach and Schön (2011), the clock constraints are selected depending on the type of ultra-stable oscillator in use e.g. Rb, Cs frequency standards, or H maser clocks. In the common clock SD modeling approach, however, the clock stability requirement is mainly replaced by the link stability requirements, i.e. even a clock with lower frequency stability can be used provided that its signal is equally (at 1 mm accuracy) distributed to both receivers.

Assuming a batch least squares estimation for n epoch, in a first approach, the differential clock variation can be approximated by a sequence of linear polynomials, where the modeling interval Δt depends mainly on the link stability. Over the lth modeling interval $[t_{0,l}, t_{0,l} + \Delta t[$, the metric

differential receiver clock error $c\delta t_{AB,l}$ can be described as

$$c\delta t_{AB,l}(t) = \mathrm{d}_l + \mathrm{m}_l\left(t - t_{0,l}\right) \qquad (3)$$

with the corresponding (clock phase) offset d_i, (clock phase) drift m_i and subsequent continuity constraints:

$$\mathrm{d}_l + \mathrm{m}_l\Delta t - \mathrm{d}_{l+1} = 0 + \varepsilon_d \quad |\sigma_d \qquad (4a)$$

$$\mathrm{m}_l - \mathrm{m}_{l+1} = 0 + \varepsilon_m \quad |\sigma_m \qquad (4b)$$

where $\varepsilon_d, \varepsilon_m$ are small inconsistencies and σ_d, σ_m the standard deviations of the constraints, cf. Weinbach (2013, p. 66ff). In a similar way, the differential tropospheric delay is estimated.

The design matrix is formed by block diagonal matrices: $\mathbf{A}_{coo,i}$ for the epochwise coordinate triple, containing the line-of-sight unit vector as partial derivatives, $\mathbf{A}_{trop,j}$ for the differential tropospheric parameters over intervals j of e.g. 2 h, and $\mathbf{A}_{clk,l}$ the part of the differential receiver clock error for the selected clock modeling intervals *l*

$$\begin{aligned}\mathbf{SD} + \mathbf{v}_{SD} &= blkdiag\left(\mathbf{A}_{coo,SD,i}\right)\mathbf{x}_{coo} \\ &+ blkdiag\left(\mathbf{A}_{trop,SD,j}\right)\mathbf{x}_{trop} \\ &+ blkdiag\left(\mathbf{A}_{clk,SD,l}\right)\mathbf{x}_{clk} \\ &= \mathbf{A}_{SD}\mathbf{x}_{SD}\end{aligned} \qquad (5)$$

In case of DD, the differential receiver clock error is eliminated by forming differences between two satellites, subsequently the design matrices for the coordinates and tropospheric delays are modified.

$$\begin{aligned}\mathbf{DD} + \mathbf{v}_{DD} &= blkdiag\left(\mathbf{A}_{coo,DD,i}\right)\mathbf{x}_{coo} \\ &+ blkdiag\left(\mathbf{A}_{trop,DD,j}\right)\mathbf{x}_{trop} \\ &= \mathbf{A}_{DD}\mathbf{x}_{DD}\end{aligned} \qquad (6)$$

Fig. 3 shows schematically the non-zero elements in the design matrices.

The stochastic model of SD is obtained by assuming an elevation dependent variance of the phase observations, and uncorrelated SD. Since no temporal correlations are considered the epochwise cofactor matrix reads:

$$\begin{aligned}\mathbf{Q}_{SD,i} &= diag\left(1/\sin^2 E_{k,A,i} + 1/\sin^2 E_{k,B,i}\right) \\ &\approx diag\left(2/\sin^2 E_{k,i}\right)\end{aligned} \qquad (7)$$

$E_{k,i}$ being the elevation of satellite *k* at epoch *i*,

which is approximately the same at both station A and B. In case of DD, the mathematical correlations induced by the use of a common reference satellite per epoch are taken into account (matrix **M**), yielding a fully populated matrix

$$\mathbf{Q}_{DD,i} = \mathbf{M}\mathbf{Q}_{SD,i}\mathbf{M}^T \qquad (8)$$

The inverse of the respective cofactor matrices is the weight matrix **P**.

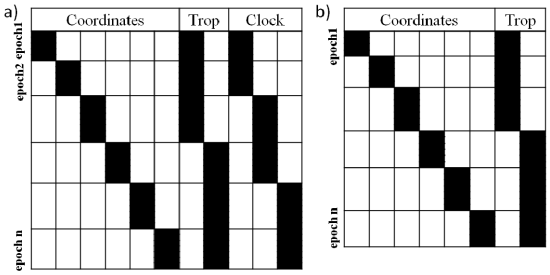

Fig. 3 Non zero-elements in the design matrices (black), Case of between-station single differences (a), same situation for DD (b).

4 Simulations

For static positioning, using common clock SD instead of DD improves significantly the height component and the tropospheric delay (80% and 60% improvement, respectively), while as expected the horizontal coordinate components are almost unchanged. However, a perfect synchronization of the two receiver clocks is mandatory. This situation totally changes when estimating even only one additional clock parameter, Then, the gain in performance for static positioning between both approaches (namely SD processing with clock modeling and DD processing) almost vanishes. This is in agreement with studies for Precise Point Positioning and single point positioning by Weinbach and Schön (2009) and Weinbach (2013). They found improvements only for kinematic analyses, i.e. when the coordinate resolution is higher than the clock resolution. The main benefit is

then a better resolution of the height component as shown by Weinbach and Schön (2015) for earthquake monitoring.

In order to analyse possible improvement for kinematic coordinate estimation in relative positioning with common clock singles differences, simulation studies are carried out for the baseline between KOP1 and MEI1 station at PTB campus. Using the real satellite geometry, a 12 h scenario is computed, with optimal conditions of 5° cut-off and the realistic conditions of 20° cut-off at this site. The data rate was 30 sec. An elevation dependent observation weighting is applied, cf. Eq.(7). A piecewise linear differential tropospheric parameter is estimated over 2 h segments. The ambiguities were assumed to be already successfully resolved. With this information, the design matrix **A** (Fig.3) is filled.

In one simulation run DD are formed, while in the second run SD are computed and a differential receiver clock error is estimated as piecewise linear parameter. The clock modeling interval is varied from 15 minutes to 6 hours. No constraints are added in order to get a rather conservative assessment of the attainable improvements. The standard DD procedure is equal to an epochwise estimation of the receiver clock, cf. Lindlohr and Wells (1985) and is thus used as reference. The most perfect but hypothetical situation is dealt with in the last simulation run, where a perfect synchronization without any need for clock estimation is considered.

The simulation focuses on the following quality parameters, which depends only on the design matrix **A** and the weight matrix **P**: (i) the mean formal standard deviation for the North, East, and Up component (ii) the vulnerability against outliers. The impact of undetected outliers on the estimated parameters is the most critical issue, since it affects the accuracy of the results. Often, concepts of data snooping are used, e.g. Baarda (1968) or Teunissen (2000). However, a more general approach is to bound the errors in the observation vector **dl** by the vector norm and assess its impact on the estimated parameter vector **x** using the triangular inequality for matrix and vector norms:

$$\|\mathbf{x}\| \le \|\mathbf{K}\|\|\mathbf{dl}\| = s_{\max}\|\mathbf{dl}\| \qquad (9)$$

where **K** is the transfer matrix from the observation space to the parameter space

$$\mathbf{K} = \left(\mathbf{A}^T\mathbf{P}\mathbf{A}\right)^{-1}\mathbf{A}^T\mathbf{P}, \qquad (10)$$

Its norm $\|\mathbf{K}\|$ should be compatible to the L2 vector norm, thus the spectral norm, i.e. the maximum singular value of **K** is selected:

$$\|\mathbf{K}\| = s_{\max} = svd_{\max}(\mathbf{K}) \qquad (11)$$

Similar formulas can be found in integrity monitoring, cf. Brown and Sturza (1990).

Table 1 gives the mean formal standard deviation of the epochwise estimated tropocentric coordinates (North, East, and Up). The standard processing with DD is used as reference, cf. first line. Comparing the different clock modeling intervals, it is obvious that clock modeling has - as expected - almost no impact on the horizontal coordinate components. However, due to the pronounced correlations between the height, receiver clock error as well as tropospheric delay (cf. Rothacher and Beutler, 1998), mainly improvements in the height component can be seen: for clock modeling intervals of 15 minutes already an improvement of 62% to the 1 mm level is obtained, thus the height component is as precise as the horizontal components. In the ideal case of perfect synchronization even 73% of reductions are reached. All further clock modeling intervals leads to improvements in between.

Tab. 1 Mean formal coordinate standard deviation when using different clock modeling intervals. A cut-off angle of 5° is applied and 2h tropospheric parameter are estimated.

	Clock Interval	$\bar{\sigma}_N$ [mm]	$\bar{\sigma}_E$ [mm]	$\bar{\sigma}_U$ [mm]
DD		1.9	1.3	2.9
SD	15'	1.8	1.2	1.1
Impr.[%]		3	6	62
SD	30'	1.8	1.2	1.0
Impr.[%]		3	6	67
SD	2 h	1.8	1.2	0.9
Impr.[%]		3	6	70
SD	6 h	1.8	1.2	0.8
Impr.[%]		3	6	73
SD	no	1.8	1.2	0.7
Impr.[%]		3	6	73

Beyond the mean values listed in Table 1, a detailed analysis of the values reveals that also epoch-by-epoch the clock modeling approach outperforms the standard DD procedure, the latter one being implicitly equal to an epochwise estimation of the receiver clock, cf. Lindlohr and Wells (1985).

In case of no estimation of tropospheric delays the height standard deviation is further improved by approximately 3%. The values of s_{max} are not listed here since for this favorable geometry only small improvements can be obtained.

This situation changes if a 20° cutoff angle is applied, cf. Table 2. Since in this case the geometry is less favourable and fewer common satellites are in view, the median of the standard deviations is computed. Again in any epoch the clock modeling approach outperforms the DD procedure. Since the geometry is less favourable for positioning and less common satellites are in view, the impact, i.e. the strengthening of the geometry, of clock modeling is even higher: 55% improvement for 15 min clock modeling intervals and up to 81% for a perfect synchronization. In addition, the same precision level can be reached as with low cut-off angle.

Tab. 2 Median of formal coordinate standard deviation when using different clock modeling intervals. A cut off angle of 20° is applied and 2h tropospheric parameter are estimated.

	Clock Interval	$med\sigma_N$ [mm]	$med\sigma_E$ [mm]	$med\sigma_U$ [mm]	s_{max} [-]
DD		2.0	1.4	4.1	5500
SD	15'	2.0	1.3	1.8	662
Impr.[%]		3	6	55	87
SD	30'	2.0	1.3	1.6	251
Impr.[%]		4	9	60	95
SD	2 h	1.9	1.3	1.3	14
Impr.[%]		5	9	67	99
SD	6 h	1.9	1.2	1.0	12
Impr.[%]		6	9	75	99
SD	no	1.9	1.2	0.8	3
Impr.[%]		6	9	81	99

The last column of Table 2 shows the reduction of the maximum singular value and thus the impact of remaining systematic observation errors to the estimated parameters. Also here a strong improvement can be seen. In addition, it is worth noting that the standard deviation of the tropospheric delay parameters is also improved by up to 89 %.

5 Analysis of experimental data

5.1 Analysis of Common Clock Single Differences

In order to get a first impression on the signals contained in observed-minus-computed values (OMC), common-clock single differences are formed between MEI2 and KOP1 taking the data of our 2013 campaign. The nominal coordinates as well as individual and absolute phase center offsets and phase center variations (PCO/PCV) are applied. A SD ambiguity term is eliminated by rounding.

A sample 24 h SD time series for the L1 GPS signal derived from the C/A Code (RINEX3.0 GL1C) is processed. Fig 4. depicts the resulting time series, color-coded for each satellite, where blue colors indicate low and red high PRN numbers, respectively. The high frequency noise of the time series is in the order of 1-2 mm.

All time series show a common offset of approximately 0.075 m. This indicates the differential receiver clock error, including differential cable and hardware delays. Additionally, a small drift of around +5 mm over the period of one day is visible, which likely points to variations in the differential receiver clock and hardware delays.

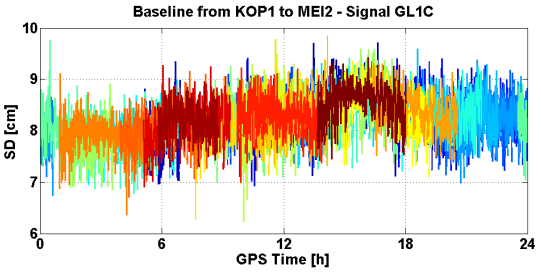

Fig. 4 24h OMC time series [m] of common clock single differences for the 290 m baseline between Kopfermann and Meitner building. Blue colors indicate satellites with low PRN, red colors with high PRN

Furthermore, a closer look to individual SD time series of each satellite reveals long periodic elevation-dependent deflections of up to 10 mm indicating a remaining tropospheric delay that is not cancelled out during single differencing of the OMC. This means that relative tropospheric delays between station KOP1 and MEI1 resulting from the height difference of 16 m can be observed in the SD. One explanation could be special atmospheric situation with one station in the forest and one above. Subsequently, a specific micro climate could be formed and the standard model will not reflect this specific situation. With typical values for the refraction index for microwaves, this impact can be assessed to 300 ppm * 16 m = 5 mm.

5.2 Kinematic Estimation of Coordinates

With this preanalysis in mind, a kinematic coordinate time series was estimated with both approaches over the first 12 h of DOY297 in 2013. We set up the differential receiver clock error as piecewise linear function cf. Eq.(3) over 6 h. In this first analysis no constraints were applied, thus conservative performance is obtained. A tropospheric zenith delay parameter is estimated as piecewise linear function of 2 h. The data rate is 30 sec and the cut-off angle 20°.

Fig. 5 shows the resulting coordinate time series for the first 7.5 h, then due to epochs with only 4 satellites in common the performance of the DD is significantly reduced. A similar performance of both processing strategies can be observed for the North and East component with typical 1-2 cm variations of the kinematic coordinates. The RMS are 1.4 (1.5) cm for North and 1.1 (1.3) cm for East for the SD (DD) processing. For the height time series, the impact of clock modeling is clearly visible: the coordinates time series is much smoother. Here the RMS is reduced from 2.4 cm (DD processing) to 1.5 cm in case of common clock SD. Thus, small high frequency variations in the height component can now be detected, too. A small jump in the time series is visible between the two clock modeling intervals at 6 o'clock. Further investigations will focus on the optimal determination of the constraints.

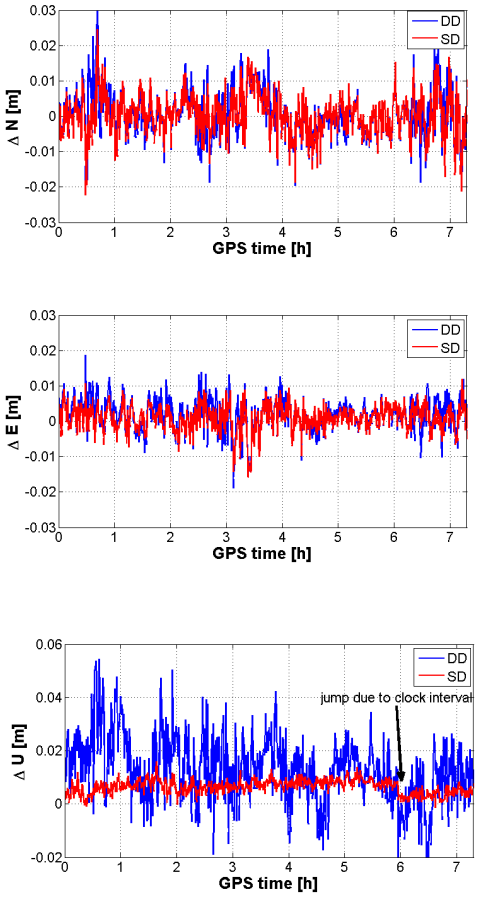

Fig. 5 Comparison of kinematic coordinates for the 290 m baseline between Kopfermann and Meitner building for the North (top), East (middle), and Up (down) component in [m]. Blue: computed with standard DD, red computed with common clock single-differences.

6 Conclusion and Outlook

An interesting and valuable GNSS common clock data set at PTB campus has been analysed. The set-up shows the current potential of the common clock analysis strategy but also the challenges. The main findings are:

Perfect synchronization in a common clock set-up with remotely operated receivers is very difficult to achieve, due to asymmetries in the receivers themselves and in the signal distribution equipment, and temperature effects acting on antenna cables (outdoor) and installed equipment (indoor). Thus, only little advantage of common clock SD for static analyses can be obtained.

However, significant impact for kinematic analyses can be achieved for the height component due to the high correlations with the receiver clock (reduction of the standard deviation of up to 70%). Furthermore, the impact of remaining systematic errors in the observations is reduced thanks to a strengthened geometry of the positioning.

Consequently, benefits for fixed installed GPS based monitoring systems have been identified, in particular if the height component and a high rate date are of interest. Further studies are needed to improve the methodology.

Acknowledgement

We gratefully acknowledge funding from the European Metrology Research Program (EMRP). The EMRP is jointly funded by the EMRP participating countries within EURAMET and the European Union. The authors thank Thomas Krawinkel (IfE) for technical support during the experiments.

References

Avallone, A., M. Marzario, A. Cirella, A. Piatanesi, A. Rovelli, C. Di Alessandro, E. D'Anastasio, N. D'Agostino, R. Giuliani, M. Mattone (2011): Very high rate (10 Hz) GPS seismology for moderate-magnitude earthquakes: The case of the Mw 6.3 L'Aquila (central Italy) event, *J.Geophys. Res.*, 116, B02305

Baarda, W. (1968): A Testing Procedure for Use in Geodetic Networks. *Neth. Geod. Comm. Publ. on Geodesy*, new series, Vol. 2, No. 5, Delft.

Bischof C., and S. Schön (2013): Performance Evaluation of Different High-Rate GPS Receivers under Various Dynamic Stress Scenarios, *Proceedings of the European Navigation Conference (ENC) 2013*, April 23.-25., Vienna, Austria

Brown, A., and M. Sturza (1990); The Effect of Geometry on Integrity Monitoring Performance. *Presented at the Institute of Navigation Annual Meeting,* June 1990

Brückl, E., Brunner, F.K., Lang. E, Mertl, S., Müller, M., U. Stary (2013): The Gradenbach Observatory—monitoring deep-seated gravitational slope deformation by geodetic, hydrological, and seismological methods. *Landslides* 10:815–829

Häberling, S., Rothacher, M., Zhang, Y., Clinton, J., A. Geiger (2015): Assessment of high-rate GPS using a single-axis shake table. *Journal of Geodesy* 89(7):697-709

Kim, D., Langley, R., Bond, J., A. Chranowski (2003): Local deformation monitoring using GPS in an open pit mine: initial study. *GPS Solutions*. 7:176-185.

Krawinkel T., Schön S. (2015): Benefits of receiver clock modeling in code-based GNSS navigation*, GPS Solutions* online first. DOI: 10.1007/s10291-015-0480-2

Larson, K. M. (2009), GPS seismology, *J. Geod.,* 83(3), 227–233.

Leute, J, Bauch, A., Krawinkel, T., S. Schön (2016): Common clock GNSS-baselines at PTB. this conference

Li, X., Ge, L., Ambikairajah, E., Rizos, C. Y. Tamura (2005): Analysis of Seismis Response of a Tall Tower Monitored with an Integrated GPS and Accelerometer System. *J. Geospatial Eng.* 7(1):30-38

Lindlohr, W., and D. Wells (1985) GPS design using undifferenced carrier beat phase observations *manuscripta geodaetica* 10: 255-295

Macias-Valadez, D., Santerre, R., Larochelle, S., R. Landry (2012). Improving vertical GPS precision with a GPS-over-fiber architecture and real-time relative delay calibration. *GPS Solutions*, 16(4):449–462.

Malet, J.-P., Maquaire, O., E. Calais (2002): The use of Global Positioning System for the continuous monitoring of landslides. Application to the Super-Sauze earthflow (Alpes-de-Haute-Provence, France). *Geomorphology,* 43: 33-54.

Moschas, F., and S. Stiros (2014). PLL bandwidth and noise in 100 Hz GPS measurements. *GPS Solutions*, 19(2), 173-185.

Moschas, F., and S. Stiros, (2015). Dynamic Deflections of a Stiff Footbridge Using 100-Hz GNSS and Accelerometer Data. *Journal of Surveying Engineering*, 04015003.

Pollinger F. et al. (2015), Metrology for Long Distance Surveying: A Joint Attempt to Improve Traceability of Long Distance Measurements. *IAG 150 Years - Proceedings of the 2013 IAG Scientific Assembly, Potsdam, Germany, 1-6 September, 2013, International Association of Geodesy Symposia, Vol. 143, Springer International Publishing Switzerland, doi: 10.1007/1345_2015_154*

Ray, J. and K. Senior (2003): IGS/BIPM pilot project: GPS carrier phase for time/frequency transfer and timescale formation. *Metrologia*, 40(3):270-288.

Roberts, G. W., Dodson, A. H., Ashkenazi, V., Brown, C. J., R. Karuna (1999): Comparison of GPS Measurements and Finite, *Proc.ION GPS 1999*, Nashville, TN, September 1999, pp. 79-84.

Rothacher, M., and G. Beutler (1998). The role of GPS in the study of global change. *Physics and Chemistry of The Earth,* 23(9-10):1029–1040.

Santerre, R. and G. Beutler (1993). A proposed GPS method with multi-antennae and single receiver. *Bulletin Géodésique*, 67:210–223.

Schön S., A. Wieser und K. Macheiner (2005): Accurate tropospheric correction for local GPS monitoring networks with large height differences*. Proc. ION GNSS 2005*, 250-260.

Teunissen P. (2000): *Testing Theory: an Introduction* . Series on Mathematical Geodesy and Positioning, Delft University Press, Delft University of Technology, Delft, The Netherland

Wang, K., and M. Rothacher (2013): Stochastic modeling of high-stability ground clocks in GPS analysis, *J. Geod.*, 87(5), 427–437.

Weinbach U. and S. Schön (2009): Evaluation of the clock stability of geodetic GPS receivers connected to an external oscillator*, Proc. ION GNSS 2009*, Savannah, GA, USA, 22-25 September 2009, 3317-3328

Weinbach, U., and S. Schön (2011), GNSS receiver clock modeling when using high-precision oscillators and its impact on PPP, Adv. Space Res.,47(2), 229–238.

Weinbach U. and S. Schön (2015). Improved GPS-based co-seismic displacement monitoring using high-precision oscillators. *Geophysical Research Letters* 42(10):3773-3779, 10.1002/2015GL063632

Weinbach U. (2013): Feasibility and impact of receiver clock modeling in precise GPS data analysis, *Wissenschaftliche Arbeiten der Fachrichtung Geodäsie und Geoinformatik der Leibniz Universität Hannover*, Dissertation Nr. 303.

Wieser A., Brunner F.K. (2002) Analysis of Bridge Deformations using Continuous GPS Measurements In: Kopáčik A. and Kyrinovič P. (Eds.) *INGEO 2002*, 2nd Conference of Engineering Surveying, Bratislava: 45-52. (2002)

Xu, P., Shi, C., Fang, R., Liu, J., Niu, X., Zhang, Q., Yanagidani, T., (2013) High-rate precise point positioning (PPP) to measure seismic wave motions: an experimental comparison of GPS PPP with inertial measurement units. *Journal of Geodesy* 87(4):361-372